Dynamics of water, methanol, and ethanol in a room temperature ionic liquid

Patrick L. Kramer, Chiara H. Giammanco, and Michael D. Fayer[a)]
Department of Chemistry, Stanford University, Stanford, California 94305, USA

(Received 5 January 2015; accepted 13 February 2015; published online 18 March 2015)

The dynamics of a series of small molecule probes with increasing alkyl chain length: water, methanol, and ethanol, diluted to low concentration in the room temperature ionic liquid 1-ethyl-3-methylimidazolium bis(trifluoromethylsulfonyl)imide, was investigated with 2D infrared vibrational echo (2D IR) spectroscopy and polarization resolved pump-probe (PP) experiments on the deuterated hydroxyl (O–D) stretching mode of each of the solutes. The long timescale spectral diffusion observed by 2D IR, capturing complete loss of vibrational frequency correlation through structural fluctuation of the medium, shows a clear but not dramatic slowing as the probe alkyl chain length is increased: 23 ps for water, 28 ps for methanol, and 34 ps for ethanol. Although in each case, only a single population of hydroxyl oscillators contributes to the infrared line shapes, the isotropic pump-probe decays (normally caused by population relaxation) are markedly nonexponential at short times. The early time features correspond to the timescales of the fast spectral diffusion measured with 2D IR. These fast isotropic pump-probe decays are produced by unequal pumping of the OD absorption band to a nonequilibrium frequency dependent population distribution caused by significant non-Condon effects. Orientational correlation functions for these three systems, obtained from pump-probe anisotropy decays, display several periods of restricted angular motion (wobbling-in-a-cone) followed by complete orientational randomization. The cone half-angles, which characterize the angular potential, become larger as the experimental frequency moves to the blue. These results indicate weakening of the angular potential with decreasing hydrogen bond strength. The slowest components of the orientational anisotropy decays are frequency-independent and correspond to the complete orientational randomization of the solute molecule. These components slow appreciably with increasing chain length: 25 ps for water, 42 ps for methanol, and 88 ps for ethanol. The shape and volume of the probe, therefore, impact reorientation far more severely than they do spectral diffusion at long times, though these two processes occur on similar timescales at earlier times. © *2015 AIP Publishing LLC.* [http://dx.doi.org/10.1063/1.4914156]

I. INTRODUCTION

Room temperature ionic liquids (RTILs) have emerged as an important class of solvents with a wide array of currently realized and potential applications[1] in synthesis and catalysis,[2,3] (bio) materials processing,[4–7] separations,[5] and energy technologies.[8,9] The huge library of cations and anions that can be assembled into ionic liquids (allowing at least one million simple ILs with a single cation and anion[1]) has led to their designation as designer solvents. The choice of an existing RTIL or synthesis of a new material for a specific purpose is guided by relationships between ionic liquid molecular structure and properties with respect to the task.

One particularly powerful and easily tunable facet is the set of hydrogen bonding interactions between ionic liquids and species in solution.[10,11] Such interactions occur between an ion and solute or among the RTIL's constituent cations and anions.[12] The importance of the hydrogen bond (H-bond) in chemistry and biology cannot be overstated.[13,14] From small molecule solutes to large biological structures, a wide range of species will undergo hydrogen bonding within an ionic liquid. Protic ionic liquids (as opposed to the aprotic material studied here) have properties dominated by the hydrogen bonds between cation and anion.[12] More generally, because most ionic liquids are hygroscopic,[10,15] water is an inevitable co-solvent in nearly any ionic liquid system that has not been rigorously dried and handled with impeccable air-free technique, a level of care usually reserved for small volume samples in fundamental studies. Water's effect on RTIL properties will inevitably depend on the hydrogen bonds it forms,[10] hence it is reasonable to believe that the hydrogen bonding ability of a RTIL is one of the major points in determining its usefulness in a particular application.

Infrared (IR) spectroscopy is a very useful approach for observing hydrogen bonded structures and dynamics.[16–18] As a vibrational probe, we focus in this paper on the hydroxyl group as a hydrogen bond donor, though others are also important, e.g., the N–H group in peptides.[19] The great sensitivity of IR techniques to hydrogen bonds results from the close correlation between the number and strength of H-bonds and the hydroxyl stretch frequency.[20–22] Stronger and shorter hydrogen bonds are identified by lower frequencies, while

[a)]Author to whom correspondence should be addressed. Electronic mail: fayer@stanford.edu

 © 2015 AIP Publishing LLC

This article is copyrighted as indicated in the article. Reuse of AIP content is subject to the terms at: http://scitation.aip.org/termsconditions. Downloaded to IP: 171.64.123.74 On: Wed, 18 Mar 2015 16:17:11

weaker and longer H-bonds correspond to higher frequencies. The vibration of interest in this study is the O–D (deuteroxyl) stretch, chosen for experimental convenience.[20] Molecular Dynamics (MD) simulations have demonstrated that the O–D stretch reports on the same hydrogen bond properties as the O–H stretch in systems such as bulk water (5% HOD, singly deuterated water, in H_2O).[22] Therefore, the hydrogen bond dynamics measured for the O–D of HOD are assumed to be essentially the same as those felt by the hydroxyl (O–H) of water molecules in the RTIL. We extend this assumption to the hydroxyl stretch of small alcohols as well.

The Fourier transform IR (FT-IR) studies of water in a variety of ionic liquids have identified the overall hydrogen bonding motifs.[10] At low water concentrations, water molecules are isolated from each other, with each hydroxyl donating a hydrogen bond to a different anion, that is, bridging two anions. At higher water concentrations, clusters of hydrogen bonded water molecules form. Similar trends have been identified for methanol in an ionic liquid,[23] with the isolated alcohol H-bonding to a single anion when dilute and forming oligomers as the concentration increases. These investigations, however, have revealed only the time-averaged hydrogen bonding properties. Because hydrogen bonds are highly dynamic, fluctuating entities, a full understanding of their properties will include the motions on their natural timescales: from tens of femtoseconds up to nearly 100 ps. To gain this dynamic perspective, we have utilized ultrafast two dimensional infrared (2D IR) and polarization selective infrared pump-probe (PP) spectroscopy to investigate hydrogen-bonded structure evolution. A recent study[24] using these techniques to probe HOD and D_2O isolated in a room temperature ionic liquid, 1-butyl-3-methylimidazolium hexafluorophosphate ($BmimPF_6$), supported the general picture of water-RTIL interactions summarized above and found several timescales of hydrogen bond fluctuations determining the orientational and spectral diffusion rates. MD simulations have further decomposed the OD of HOD spectral diffusion dynamics into largely translational motion between water and anion species, with almost no contribution from cation dynamics,[25] as expected for the model of hydroxyl groups interacting primarily through H-bonds with anions in a RTIL.[10]

We have characterized the hydrogen bonding dynamics of water, methanol, and ethanol, a series of small molecule vibrational probes of increasing length, isolated in the RTIL, 1-ethyl-3-methylimidazolium bis(trifluoromethylsulfonyl)imide ($EmimNTf_2$), a hydrophobic, low-melting, relatively low-viscosity, and highly stable material.[9,26] Due to the short cation chain length, this RTIL is not believed to have significant polar-apolar segregation.[27,28] The vibrational probe isolation is in the sense that no water-water or alcohol-alcohol hydrogen bonds form; the solutes are at low enough concentration that only ion-probe interactions occur. The resulting spectral simplification allows us to focus on the fundamental hydrogen bond dynamics between these probes and $EmimNTf_2$ without the added complication of hydroxyl oligomer contributions. Our measurements of spectral diffusion (capturing the fluctuations in hydrogen bond structure) and reorientational motion (tracking directly the angular fluctuations of the O–D transition dipole) both report a clear slowing of hydrogen bond motion as the alkyl chain length of the probe increases to approach the 2 carbon chain of the $Emim^+$ cation. As the vibrational probe molecule increases in length, the slowing of the orientational relaxation is more dramatic than that of the spectral diffusion. It was found that the ultrafast IR techniques are sensitive to a dynamic discrimination by the RTIL $EmimNTf_2$ between solute molecules of similar functionality but differing shape and volume. Such solute structure-dependent dynamics may have important consequences for separations and synthetic procedures conducted in an ionic liquid medium.

The paper is organized as follows. Section II gives a brief overview of the ultrafast infrared techniques and sample preparation procedures. Section III presents the linear IR line shapes for the three samples of interest, which will be examined in more detail by the nonlinear IR experiments. In Sec. IV, the 2D IR spectra are presented and the frequency-frequency correlation function (FFCF) for each probe is obtained. The isotropic (population) decays from the PP experiments are discussed in Sec. V. The strikingly nonexponential, wavelength-dependent population decays are decomposed into contributions both from the true population relaxation (at long time) and spectral diffusion (at short time). The presence of spectral diffusion in an observable regarded commonly as the pure population dynamics is explained using breakdown of the Condon approximation and by analogy to a narrowband pump transient hole-burning experiment. Because the pure population decay lifetimes have only a small wavelength dependence, it is concluded that the vibrational bands are composed of a single population of hydroxyl oscillators that are dynamically inhomogeneously broadened by the distribution of local hydroxyl H-bond environments. Section VI treats the pump-probe orientational anisotropy (orientational correlation function) decays. Again, these curves are highly nonexponential and wavelength dependent. Because the dynamics are assigned to a single hydroxyl population, the multiple exponential timescales are modeled by periods of restricted angular diffusion (wobbling-in-a-cone) followed by free diffusion for complete angular randomization. In Sec. VII, the spectral diffusion and orientational dynamics are compared and a picture of the hydrogen bond and solvating ion motions in a RTIL is developed. Concluding remarks are given in Sec. VIII. A modification of the wobbling-in-a-cone model, incorporating three cones for restricted angular motion, is presented in the supplementary material.[29]

II. EXPERIMENTAL PROCEDURES

A. Laser system

The femtosecond laser system and 2D IR/PP interferometer used in this work have been described in detail previously,[30] along with the theoretical background of polarization-selective pump-probe[31,32] (transient absorption) and 2D infrared spectroscopy.[33,34] Briefly, a Ti:Sapphire oscillator seeds a regenerative amplifier that outputs 600 μJ pulses at 1 kHz, with approximately 42 fs full width at half maximum (FWHM) duration and 800 nm center frequency. The regen output pumps an optical parametric amplifier/difference frequency system resulting in mid-IR

This article is copyrighted as indicated in the article. Reuse of AIP content is subject to the terms at: http://scitation.aip.org/termsconditions. Downloaded to IP: 171.64.123.74 On: Wed, 18 Mar 2015 16:17:11

pulses centered at ~3.8 μm (tuned to match the O–D absorption peak of interest), with a bandwidth of ~220 cm^{-1} and pulse energy of ~4 μJ. Germanium and calcium fluoride (CaF_2) plates are used to compensate for dispersion, yielding nearly transform-limited 60 fs FWHM pulses in the sample.

B. 2D IR spectroscopy

For the 2D IR experiment, the IR pulse is split into 4 replicas, denoted pulses 1, 2, 3, and local oscillator (LO). All pulses are horizontally polarized. Pulses 1, 2, and 3 are crossed in the sample in the box-CARS geometry. The vibrational echo is emitted in the phase-matched direction and is overlapped spatially with the LO following the sample for heterodyne detection. Pulse 3 is chopped allowing subtraction of the LO spectrum from the heterodyne signal and correction for its finite bandwidth. Variable delays between the pulses are obtained with precision translation stages in the 1, 2, and LO beam paths. The delay between pulses 1 and 2, the first coherence period, is denoted τ, that between 2 and 3, the population period, is T_w, and the observation time following pulse 3, the final coherence period, is t. The echo and local oscillator pulses are temporally overlapped by adjusting the delay of the LO with respect to pulse 3. The heterodyned signal is dispersed with a monochromator acting as a spectrograph and detected on a liquid nitrogen cooled 32-element mercury cadmium telluride (MCT) array. The FT with respect to t, performed by the spectrograph, gives the vertical, ω_m, axis of a 2D spectrum. At a fixed T_w, the delay τ is scanned to produce an interferogram. A numerical FT along τ then gives the horizontal, ω_τ, axis. A 2D spectrum is collected for each of a series of waiting times T_w. A 2D IR spectrum correlates the initial oscillation frequency ω_τ with the final frequency ω_m, after a particular waiting time T_w.

In a 2D IR experiment, T_w is fixed and τ is scanned to produce a 2D spectrum. Then, T_w is increased and another spectrum is obtained. The dynamical information is contained in the change in shape of the 2D spectrum with T_w. The change in shape of the 2D IR spectrum as a function of T_w is caused by spectral diffusion, which reports on the structural dynamics. Inhomogeneous broadening of the O–D stretch spectrum (see Figure 1) gives rise to a range of transition frequencies. The liquid structure interacting with an individual molecular vibration determines the center frequency of its Lorentzian line, which is produced by homogeneous broadening. The total absorption line is the convolution of the individual molecules' Lorentzians with an essentially Gaussian distribution of center frequencies. Structural evolution of the medium causes the vibrational frequencies to changes. Thus, as the liquid structure changes, the frequency of a particular molecule will change in time (spectral diffusion). At sufficiently long T_w, the vibrational probe will have sampled all liquid structures; hence, all of the frequencies present in the inhomogeneously broadened FT-IR absorption spectrum will have been sampled as well.

In effect, the first and second pulses of the vibrational echo pulse sequence "label" the initial vibrational probe frequencies. Then, during T_w, the waiting time between pulse 2 and 3, the structure of the liquid evolves, causing the vibrational frequencies to shift. This period is ended by the arrival of the third pulse, which also stimulates the emission of the vibrational echo pulse. The echo contains information on the final frequencies of the vibrational oscillators. When T_w is short, the structure of the liquid is relatively unchanged from when the vibrations were first labeled, producing final frequencies that differ little from the starting frequencies. At longer T_w, the liquid structure has had more time to evolve and the final frequencies are less correlated with the initial frequencies. The loss of correlation as T_w increases is manifested as a change in shape of the 2D IR spectrum. At short T_w, the 0–1 portion of the 2D IR spectrum is elongated along the diagonal (the 45° line with positive slope that bisects the vertical and horizontal frequency axes). As T_w increases and frequencies are less correlated, the shape of the spectrum becomes more symmetrical. If all of the environments are sampled within the experimental time window, which is limited by the vibrational lifetime, the spectrum becomes round. Thus, the structural dynamics of the liquid can be extracted from the change in shape of the 2D IR spectra as a function of T_w.

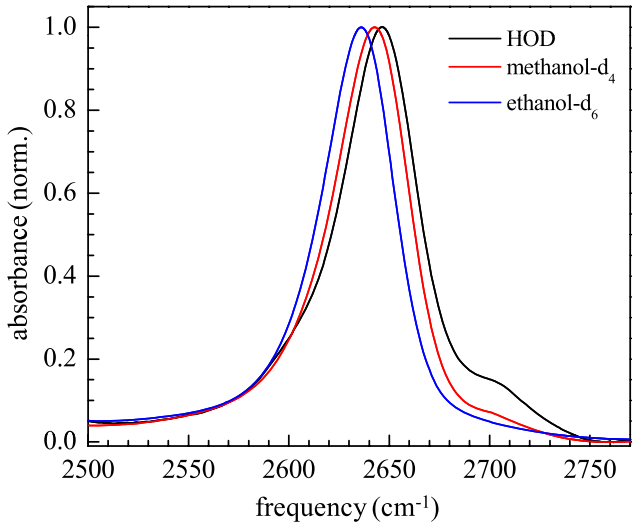

FIG. 1. Normalized, background-subtracted FT-IR spectra of HOD (30% in H_2O), methanol-d_4, and ethanol-d_6 in $EmimNTf_2$ at ion pair to probe ratios of 18:1, 21:1, and 19:1, respectively. The 18:1 ratio for HOD includes all water molecules in the mixture.

C. Polarization selective pump-probe experiments

In the polarization selective pump-probe experiment, the entire mid-IR pulse is split into two replicas with intensity ratio of about 90:10, denoted pump and probe, respectively. The delay between pump and probe, t, is varied by adjusting the delay on the pump path using a precision translation stage while the probe path remains fixed. The pump is chopped allowing subtraction of the probe spectrum from the PP signal. The signal is further divided by this probe spectrum to account for its finite bandwidth and the absorption by the sample. The polarization of the probe is maintained horizontal to the table. A half wave plate and polarizer set the pump to 45° relative to the probe. Following the sample, the probe pulse is resolved either parallel or perpendicular to the polarization of the pump using a polarizer in a computer controlled rotation mount. The

This article is copyrighted as indicated in the article. Reuse of AIP content is subject to the terms at: http://scitation.aip.org/termsconditions. Downloaded to IP: 171.64.123.74 On: Wed, 18 Mar 2015 16:17:11

two signals, measuring a transient change in absorbance, are denoted $I_{||}$ and $I_{\perp}$, respectively. Both parallel and perpendicular signals are projected back to horizontal polarization using a second resolving polarizer, to ensure that the probe pulse detected in either resolving configurations is of equal intensity on the array in the absence of the pump. The transmitted probe is detected with the same spectrograph and MCT array as in the 2D IR experiment. Pump-probe decays are collected by moving the resolving polarizer to either the parallel or perpendicular position and accumulating a series of t points.

D. Sample preparation

The ionic liquid $EmimNTf_2$ was obtained from IoLiTec and stored in a nitrogen atmosphere glove box. The water content was determined to be less than 45 ppm by coulometric Karl Fischer titration (Mettler Toledo). A solution of HOD in water was prepared by mixing 15% D_2O by mass with H_2O. Empirically, this ratio was found to give an acceptable compromise between maximizing the HOD concentration (and therefore signal in nonlinear spectroscopic experiments) and minimizing residual D_2O. We study the O–D stretch rather than the O–H stretch because the OD stretch has a longer vibrational lifetime. This solution of roughly 30% HOD will be referred to simply as HOD. The alcohols, methanol-d_4 and ethanol-d_6, were obtained from Sigma Aldrich in sealed ampoules. Perdeuterated alcohols were used rather than those with only O–D isotopic labeling because the vibrational lifetime of the O–D stretch was found to be longer for the perdeuterated molecules, extending our experimental observation time window. These three vibrational probes will be referred to as simply water, methanol, and ethanol where there is no risk of confusion. To prevent the uptake of excess water during sample preparation, a quantity of dry $EmimNTf_2$ was transferred to a box purged with dry air (less than 0.1% relative humidity) and all sample manipulation was conducted in this atmosphere.

HOD, methanol-d_4, and ethanol-d_6 were added to $EmimNTf_2$ to achieve mole ratios of about 20:1 ion pairs to probe molecules. It is important to note that in the case of HOD, all "water" molecules are included in this 20:1 measurement, regardless of isotopic labeling pattern. A sample of about 20:1 $EmimNTf_2$ to pure H_2O was also prepared. At these concentrations, the water or alcohol molecules are isolated, in the sense that essentially all solutes encounter only cations and/or anions as nearest neighbors and no oligomers form.[10] The precise concentration of solute is of no particular importance under these conditions, as small increases or decreases in the probe concentration will not alter the local environment observed by the infrared experiments. Even at somewhat greater water concentrations (down to 10:1 ion pairs to probes), there are no detectable oligomer contributions to the IR spectrum.

Sample cells for infrared spectroscopy were assembled using a Teflon spacer sandwiched between two 3 mm CaF_2 windows and held in a custom-machined mount. Cells with HOD and H_2O in $EmimNTf_2$ were prepared with a spacer thickness of 360 μm. Those of the neat RTIL as well as those with methanol-d_4 and ethanol-d_6 in $EmimNTf_2$ used a 150 μm thick spacer. Linear absorption spectra were recorded with a FT-IR spectrometer (Thermo Nicolet 6700).

III. LINEAR IR SPECTROSCOPY

Linear infrared (FT-IR) spectra were obtained for samples of $EmimNTf_2$ with and without the vibrational probe of interest, using the same path length in the sample cell. A sample of neat $EmimNTf_2$ served as the background for the methanol-d_4 and ethanol-d_6 containing samples. As water is present beyond the observed HOD, the "water" sample required a background that contained only H_2O as the solute. Background-subtracted and normalized FT-IR spectra of the three hydrogen bond probes in $EmimNTf_2$ are shown in Fig. 1.

The center (peak) frequencies and FWHM of the line shapes appear in Table I. As the probe is lengthened, from water to methanol to ethanol, a systematic red shift is observed while the linewidth remains nearly unchanged, narrowing only slightly. Often a red shift for hydroxyl oscillators indicates strengthening and shortening of the hydrogen bond it participates in, but the series presented here is of probe molecules with slightly different electronic structure owing to the difference in alkyl chains. Under these circumstances, a shift of center frequency does not necessarily give any information about the H-bond strength. In fact, gas phase infrared spectra of HOD, methanol, and ethanol display the same trend in center positions. There are no hydrogen bonds possible for these isolated molecules in a gas, so we conclude that there is no obvious difference in H-bond strength between the three probe molecules in this RTIL, given the linear spectrum alone.

An informative comparison is between the spectral parameters in Table I and those of bulk water, that is, the O–D stretch of dilute HOD in H_2O. This infrared spectrum has its center at 2509 cm^{-1} and a FWHM of about 170 cm^{-1}.[20] The large blue shift and narrowing in the spectrum of HOD in $EmimNTf_2$, as compared to HOD in bulk H_2O, indicates much weaker hydrogen bonding in the RTIL and a smaller range of frequencies (inhomogeneous broadening) possibly related to a smaller range of H-bond strengths. The alcohols, methanol and ethanol, also have comparatively weak hydrogen bonds. These relatively blue center frequencies and narrow linewidths confirm that we are observing water/alcohol monomers, with no significant concentration of oligomers.[10,35]

The shoulder appearing at 2704 cm^{-1}, most prominently with HOD and to a lesser extent with methanol, is the antisymmetric stretch of a small concentration of residual D_2O. There is a corresponding smaller peak, the symmetric stretch, at 2604 cm^{-1}. As mentioned in Sec. II B, the sample of nominally 30% HOD in H_2O will contain a relatively low

TABLE I. Static spectral parameters.

Solute	Center (cm^{-1})	FWHM (cm^{-1})	Anharmonicity (cm^{-1})
HOD	2645.9 ± 0.5	46.2 ± 0.5	95.9 ± 0.5
Methanol-d_4	2643.0 ± 0.5	45.4 ± 0.5	95.4 ± 0.5
Ethanol-d_6	2636.3 ± 0.5	43.3 ± 0.5	94.2 ± 0.5

This article is copyrighted as indicated in the article. Reuse of AIP content is subject to the terms at: http://scitation.aip.org/termsconditions. Downloaded to IP: 171.64.123.74 On: Wed, 18 Mar 2015 16:17:11

D_2O concentration. The appearance of D_2O in the spectrum of a perdeuterated alcohol in the ionic liquid comes from a small water impurity in the sample. Because the concentration of deuteroxyl groups is much higher than that of H_2O molecules, D/H exchange occurs producing a very small amount of D_2O and some protonated alcohol, which contributes a very small O–H stretch peak to the FT-IR spectra (not shown). The small amplitude of the D_2O peaks (particularly the symmetric stretch) and the shift from the O–D peak of interest mean their presence does not affect the analysis of IR observables.

A final feature of the infrared line shape merits attention: the bands are noticeably asymmetric, with a tail extending to the red side. One possible reason for the red tail is a greater population of structural configurations that give rise to lower frequency vibrations. The second possible mechanism is that the transition dipole is a function of frequency; this situation is commonly referred to as a non-Condon effect.[36,37] The linear spectrum's value is determined both by the population and square of the transition dipole moment at any particular frequency.[38] Non-Condon effects will be discussed further in Sec. V in the context of the multi-exponential isotropic pump-probe decays.

IV. SPECTRAL DIFFUSION: 2D IR MEASUREMENTS

Two-dimensional infrared spectra were recorded with the waiting time, T_w, in the range of 160 fs to 60 ps. Shorter waiting times are contaminated by a non-resonant electronic signal[39] (coherent artifact) originating from the liquid sample and/or the CaF_2 windows. The longest waiting time accessible was limited by both the total heterodyned nonlinear signal at short time (a function of the transition dipole strength of the O–D stretch and the probe concentration) and by the vibrational lifetime (Sec. V). HOD had a lower concentration in the RTIL (at constant ion to solute ratio) than methanol-d_4 and ethanol-d_6 to avoid the presence of excess D_2O, but its longer vibrational lifetime allowed roughly equivalent signals to those produced by the more concentrated alcohols at long times of up to 60 ps.

A representative series of 2D IR spectra at the waiting times 300 fs, 4 ps, and 30 ps are shown for methanol in Figure 2. 2D IR data for water and ethanol have very similar appearances. Two bands are visible: the 0-1 transition on the diagonal (dashed line in top panel) and the negative-going 1-2 transition shifted to lower frequency in ω_m by the vibrational anharmonicity. A fit to the 2D spectrum with tilted two-dimensional Gaussian line shapes enabled an accurate extraction of the anharmonicity (Table I). The analysis which follows will address the dynamics using the 0-1 band; the 1-2 band, in general, reports the identical dynamics.[40]

The two-dimensional line shapes in Figure 2 evolve with increasing T_w, starting with a large amount of correlation along the diagonal at short waiting time (elongation along the diagonal) and becoming more round as time progresses. This loss of correlation of initial and final frequencies in the 2D IR spectra is caused by spectral diffusion. In the long time limit, the 2D spectrum becomes the direct product of the linear absorption spectrum across both axes:[41] all frequency correlation is lost.

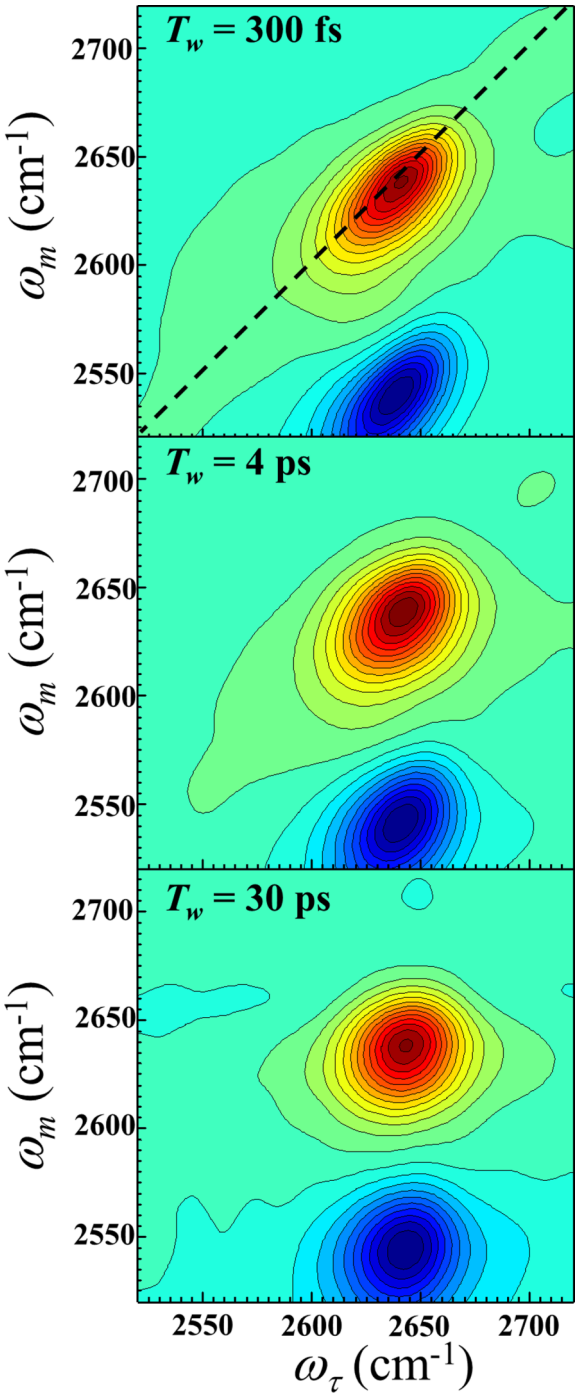

FIG. 2. Representative 2D IR spectra of methanol-d_4 in $EmimNTf_2$ at waiting times T_w = 300 fs, 4 ps, and 30 ps. The dashed line in the top panel is the diagonal. Spectral diffusion causes the spectrum, which is initially elongated along the diagonal, to become increasingly round as T_w increases. The 2D IR spectra of the other samples have very similar appearances.

We characterize the time dependence of the extent of spectral diffusion (loss of frequency correlation) using the center line slope (CLS) method.[40,42] The CLS-ω_m version of the technique is used in the present work.[42] The CLS-ω_m (henceforth referred to as CLS) is equal the T_w-dependent part of the normalized frequency-frequency correlation function, $C(t) = \langle \delta\omega(t)\delta\omega(0)\rangle$. Center line slope values were calculated from the 2D spectra for water, methanol, and ethanol at waiting times between 160 fs and 60 ps. The resulting decay data

This article is copyrighted as indicated in the article. Reuse of AIP content is subject to the terms at: http://scitation.aip.org/termsconditions. Downloaded to IP: 171.64.123.74 On: Wed, 18 Mar 2015 16:17:11

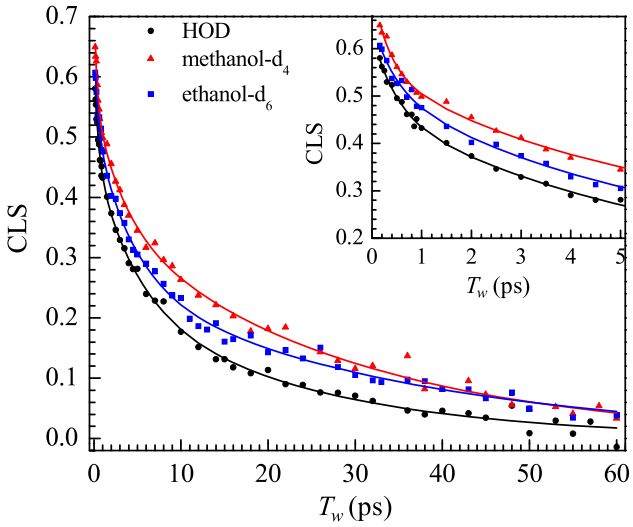

FIG. 3. Decay of the CLS for HOD (black circles), methanol-d_4 (red triangles), and ethanol-d_6 (blue squares) in the ionic liquid. Solid lines are triexponential fits to the data. The inset shows the same data and fits at short waiting times (to 5 ps).

(symbols) are plotted in Figure 3. The inset shows an expanded view of the short time portion of the CLS decay curves.

The CLS curves begin at value around 0.6-0.65 for all three solutes, and were fit with triexponential decay functions (solid curves). Single and biexponential fits could not adequately capture the early time behavior of the curves. By 60 ps, the CLS decays have almost reached zero; thus, there are no slower timescales of the frequency fluctuations beyond those obtained from the triexponential fits. Table II gives the time constant values of the triexponential fits. The first two timescales of the frequency fluctuation are very similar for the three vibrational probes: ~400 fs and ~4 ps. Within experimental error, these time constants are the same. Differences emerge on the longer timescale of tens of picoseconds. There is a steady progression toward slower spectral diffusion with increasing alkyl chain length on the solute: 23 ps for water, 28 ps for methanol, and 34 ps for ethanol.

The CLS gives the normalized FFCF, but the CLS method[40,42] additionally allows extraction of the complete FFCF, which includes the frequency fluctuation amplitudes and the homogeneous linewidth. The FFCF was modeled with the form

$$C(t) = \langle \delta\omega(t)\delta\omega(0)\rangle = \frac{\delta(t)}{T_2} + \sum_i \Delta_i^2 \exp(-t/\tau_i), \quad (1)$$

where Δ_i and τ_i are the frequency fluctuation amplitude and time constant, respectively, of the ith component. A component of the FFCF is motionally narrowed and a source of homogeneous broadening in the absorption line if $\Delta\tau < 1$. In this instance, it is not possible to determine Δ and τ separately. The motionally narrowed contribution to the absorption spectrum has a pure dephasing linewidth given by $\Gamma^* = \Delta^2\tau = 1/\pi T_2^*$, where T_2^* is the pure dephasing time. The homogeneous time that is measured, T_2, also depends on the transition dipole orientational relaxation and vibrational lifetime, and is given by

$$\frac{1}{T_2} = \frac{1}{T_2^*} + \frac{1}{2T_1} + \frac{1}{3T_{or}}, \quad (2)$$

where T_1 and T_{or} are the vibrational lifetime and orientational relaxation time. The CLS has been previously shown to be mathematically equivalent to the normalized T_w-dependent portion of the FFCF.[40,42] The homogeneous contribution and the total inhomogeneous linewidth (from the absolute value of the Δ_i's) are determined through a simultaneous fit to the T_w dependence of the CLS and the linear absorption line shape, resulting in the full FFCF (Eq. (1)).[40,42] The CLS decays have the same time constants as the FFCF and can be used to discuss the timescales of the dynamical processes in the sample. Computing the full FFCF allows these processes to be assigned their respective contributions to the linewidth.

In addition to the decay time constants, the frequency fluctuation amplitudes, homogeneous linewidths, and total dephasing times T_2 are given in Table II. The linewidth Γ is the FWHM of the Lorentzian homogeneous line. The Δ_i fluctuation amplitudes are standard deviations of the Gaussian line shape associated with each contribution to the inhomogeneous broadening. The total inhomogeneous linewidth is given by the convolution of these Gaussians, $\Delta_{total} = (\Delta_1^2 + \Delta_2^2 + \Delta_3^2)^{1/2}$. The FWHM of the total inhomogeneous line is then $2.35\Delta_{total}$. Finally, the complete linear line shape is the convolution of the homogeneous (Lorentzian) and inhomogeneous (total Gaussian) parts.

In bulk water, spectral diffusion, and therefore the FFCF, has been shown to be determined by the dynamics of hydrogen bond interactions through comparison of 2D IR data and MD simulations.[20,43] Analysis of these simulations used a map between IR absorption frequency and the electric field projected along the hydroxyl bond to calculate the FFCF from the MD trajectories. The fluctuations in hydrogen bond strength and length, and the hence hydroxyl frequencies, were well described by the field fluctuations. A similar MD study of water in the ionic liquid $BmimPF_6$ found that the frequency fluctuations were also well correlated with the electric field along the hydroxyl, and that the field fluctuations were in good agreement with the FFCF obtained from 2D IR experiments.[24,25] Therefore, the hydroxyl frequency likely

TABLE II. FFCF parameters from CLS triexponential fit and absorption line shape.

Solute	Γ (cm^{-1})	T_2 (ps)	Δ_1 (cm^{-1})	τ_1 (ps)	Δ_2 (cm^{-1})	τ_2 (ps)	Δ_3 (cm^{-1})	τ_3 (ps)
HOD	23.5	0.45	6.8 ± 0.4	0.5 ± 0.1	8.1 ± 0.5	5 ± 1	8.2 ± 0.4	23 ± 3
Methanol-d_4	12.0	0.88	7.6 ± 0.5	0.3 ± 0.1	7.9 ± 0.4	3.4 ± 0.8	10.9 ± 0.3	28 ± 1
Ethanol-d_6	14.3	0.74	6.6 ± 0.5	0.4 ± 0.1	9.4 ± 0.3	4.2 ± 0.7	9.5 ± 0.3	34 ± 3

This article is copyrighted as indicated in the article. Reuse of AIP content is subject to the terms at: http://scitation.aip.org/termsconditions. Downloaded to IP: 171.64.123.74 On: Wed, 18 Mar 2015 16:17:11

reports on similar intermolecular interactions in bulk water and when a hydroxyl containing species is solvated in an IL. Hence, it is reasonable to assume the hydrogen bonding interactions are also the major contributors to the O–D stretch frequency and spectral diffusion of hydroxyls on solutes in the ionic liquid.

The vibrational frequency of a given oscillator is determined by its hydrogen bond strength, and spectral diffusion reports on the evolution of hydrogen bonded structures which cause loss of frequency correlation. The first timescale of frequency fluctuation has a mildly smaller amplitude than the following two in each of the decays for the three vibrational probes. The fast timescales of about 300-400 fs suggest very local hydrogen bond length fluctuations between the O–D oscillator and the original H-bond acceptor. In bulk water, a 400 fs component of the spectral diffusion was shown by the MD simulations to arise mainly from hydrogen bond length fluctuations.[20,43] The second timescale process, between 3.5 and 4.5 ps, contributes somewhat more to the inhomogeneous linewidth. These dynamics likely originate from larger amplitude fluctuations around the original hydrogen bond configuration, but without major excursions of the entire probe molecule, because the timescale remains virtually unchanged in the series of water, methanol, and ethanol. The other large contribution to the inhomogeneous linewidth is from the final, long-time decay of the FFCF. As mentioned above, this timescale increases systematically from water through ethanol. It may involve both large fluctuations of the probe molecule position in the sea of ions surrounding it,[24,25] and exchange of hydrogen bond acceptor ions,[44] which would likely be accompanied by large angular jumps.[45] The mechanisms of spectral diffusion will be discussed further (Sec. VII) following the presentation of the results of the orientational relaxation measurements in Sec. VI.

V. ISOTROPIC PUMP-PROBE DECAYS AND VIBRATIONAL LIFETIMES

Using pump-probe data collected with the probe resolved parallel and perpendicular to the pump, that is, $I_{||}(t)$ and $I_{\perp}(t)$ (see Sec. II C), we can calculate the isotropic PP signal

$$P(t) = I_{||}(t) + 2\, I_{\perp}(t). \tag{3}$$

While such a signal is commonly referred to as the population decay, we will avoid this nomenclature because we show below that there are other contributions to the decay in addition to the vibrational lifetime (population decay). Pump-probe decays were obtained for the O–D stretches of water (HOD) with delay times t from 280 fs to 200 ps and methanol and ethanol with t from 280 fs to 100 ps. For each sample, typically, data for 10 different frequencies were collected across the 0-1 transition band. Four representative examples of the isotropic decay data (circles) obtained from Eq. (3) are displayed in Figure 4 for the OD stretch of HOD. The inset shows an expanded view of the short time portion of the data. The data were normalized at the first data point taken at 280 fs. The measured frequencies extend roughly equally to the red and blue sides of the peak center. Data for the other two solutes have an almost identical appearance. A small amplitude offset at long time, which is caused by a well-documented transient temperature increase of the medium following vibrational relaxation, was removed from the data at each wavelength.[46] Following approximately the first 10-20 ps for all frequencies and all samples, the isotropic signals decay as single exponential functions.

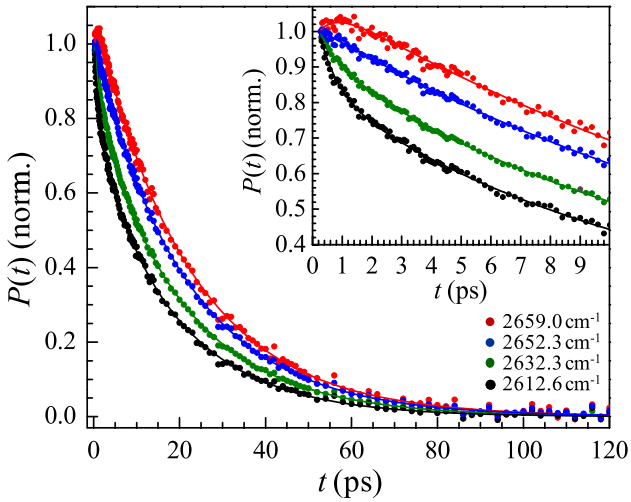

FIG. 4. Isotropic PP data for water (HOD) in EmimNTf$_2$ at representative frequencies across the absorption spectrum (points). The inset shows the early time portions of the data. The solid lines are fits with a tri-exponential function. The data are normalized at the first data point (280 fs). On the red side of the line (black), there is initially a very fast decay. On the blue side of the line (red), there is an initial fast growth. The fast components of the data are caused by spectral diffusion (see text). Data for the other two samples have very similar appearances.

As can be seen in the inset in Figure 4, at short time, the data are not decaying as a single exponential. The data at the lowest frequency (2612.6 cm^{-1}, black circles) display a rapid initial drop. In contrast, the data at the highest frequency (2659.0 cm^{-1}, red circles) have an initial increase in amplitude. The two curves at intermediate frequencies show the progression from substantial drop to an increase. The PP data require a tri-exponential function to fit the curves. This is true for all frequencies and all three samples. A tri-exponential decay, like the black curve in Figure 4, in some instances can reflect a pure population relaxation but for a sample that contains three different subensembles of molecules, each with a distinct vibrational lifetime. The IR spectra of the three species would need to overlap to such an extent that the absorption spectrum would appear as a single band. If the three spectra had somewhat different peak positions, then a wavelength dependence could be observed because at each wavelength, there would be a different amplitude contribution to the overall decay curve from the three decaying species. However, as bluer wavelengths are examined, not only do the amplitudes of the short time exponentials virtually vanish but the sign of the amplitude actually flips, so that there is a fast exponential *growth* at the bluest observed frequencies (Figure 4 inset, red circles). Furthermore, the fastest time constant is 300-400 fs. This time constant is considerably faster than the vibrational lifetime of 1.7 ps for HOD's deuteroxyl stretch in bulk water, which has a stronger hydrogen bonded network than the current systems.[46,47] The change in sign of the

This article is copyrighted as indicated in the article. Reuse of AIP content is subject to the terms at: http://scitation.aip.org/termsconditions. Downloaded to IP: 171.64.123.74 On: Wed, 18 Mar 2015 16:17:11

amplitude and the extremely fast decay both suggest that the early time behavior of the isotropic PP data is not due to the presence of multiple hydroxyl populations in the RTIL.

Pump-probe decays were recorded under identical conditions for samples that were the same but without the OD group, that is, they contained either water (H_2O) in $EmimNTf_2$ or only the ionic liquid. No signals were observed other than the ultrafast coherent artifact that tracks the pulse duration. Therefore, the fast contributions to the isotropic decays are not caused by background resonances or contaminants in the ionic liquid. Because almost identical behavior is observed using water, methanol, or ethanol as the vibrational probe, the fast signals are not caused by a contaminant associated with these solutes. These facts suggest the shape of the early time signals must originate from dynamics of the resonant OD hydroxyl probes themselves, but the isotropic PP decays are not caused solely by population relaxation.

As mentioned above, triexponential functions were necessary to adequately fit the form of the PP traces shown in Figure 4 and for all wavelengths of all three samples. In the fits for each vibrational probe, the amplitudes of the short and medium timescale components were allowed to vary, but the time constants for these terms were constrained to be the same at each frequency for a given sample. The time constant of the slowest component was allowed to vary with wavelength; the resulting variation in a given sample is small. No improvement in the fits resulted from allowing either the short time constant, medium time constant, or both to vary independently. Time constants from the global fits typically fell within the error bars of those obtained when the short and medium time constants were allowed to vary at each wavelength. The solid curves in Figure 4 and in the inset are examples of the fits. All of the fits for all wavelengths and for all three samples are equally good. We found short and medium time constants of 0.6 ± 0.1 ps and 4.5 ± 0.5 ps for water; 0.3 ± 0.1 ps and 2.8 ± 0.5 ps for methanol; and of 0.24 ± 0.1 ps and 2.3 ± 0.5 ps for ethanol. The long time decay constants are displayed in Figure 5; these will be shown to correspond to the rate of pure population relaxation (lifetimes).

The extremely rapid decays of PP signal on the red side of the spectra and growths on the blue side, with the same time constants across all wavelengths for each vibrational probe, can be understood by a mechanism in which the early time portions of the isotropic PP decays are reporting on population transfer (spectral diffusion) across the vibrational line from an initially prepared nonequilibrium distribution. A comparison of the short and medium time constants given above with the two fastest components of the spectral diffusion given in Table II shows substantial agreement. The values for water and methanol are clearly the same within experimental error. The early isotropic decay times for ethanol are slightly faster than the corresponding 2D IR measured spectral diffusion times, with the medium component somewhat outside the error bars. Nonetheless, the spectral diffusion and fast isotropic relaxation timescales are still in relatively good agreement for ethanol. We conclude that a nonequilibrium distribution of initially excited hydroxyls returns to an equilibrium distribution with the spectral diffusion rates corresponding to equilibrium dynamics.[48]

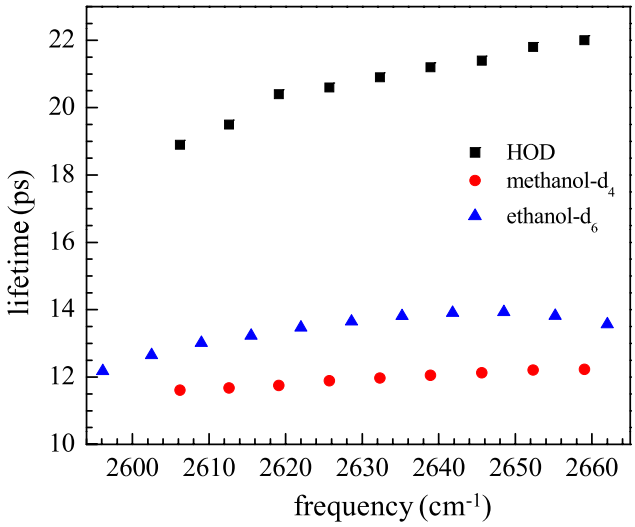

FIG. 5. Vibrational lifetimes, the slowest decay component of the isotropic pump-probe data, as a function of wavelength for HOD, methanol-d_4, and ethanol-d_6 in $EmimNTf_2$. Uncertainties in the time constants are 0.3 ps for HOD and 0.1 ps for methanol-d_4 and ethanol-d_6. The very small wavelength dependence for each sample shows that each solute is a single dynamical ensemble.

How then was this non-equilibrium distribution created? The IR frequency was tuned to the peak of the absorption spectrum for each solute, and the bandwidth of the pump pulse is so broad that its intensity can be taken to be uniform across the absorption spectrum. Thus, it was not caused by unequal pumping because of the pump spectrum. In Figure 1, the FT-IR spectra for all three solutes display wings on the red sides of the absorption lines. For HOD in bulk water, the equivalent red side wing has been attributed to non-Condon effects,[36,37] that is, the transition dipole of the absorbers becomes larger as their transition frequency shifts from blue to red. The larger transition dipole and red shift are caused by stronger hydrogen bonding. The PP data for the hydroxyl stretches of the three solute molecules studied here can be explained by assuming that there are non-Condon effects like those for the hydroxyls of water. Because molecules on the red side of the line have larger transition dipoles than those on the blue side, they are "over pumped" by the pump pulse; the number of molecules excited on the red side of the line is greater than the equilibrium number of molecules initially in the ground state with low transition frequencies relative to those on the blue of the line (high transition frequencies). Therefore, there is excess red side excited state population compared to the blue side of the line.

Spectral diffusion results in molecules changing their transition frequencies. When the excited state population is in thermal equilibrium (the number of excited states with a given transition frequency is proportional to the number of ground state molecules with that frequency), spectral diffusion causes the same number of molecules to move to the blue as move to the red, thus preserving the thermal equilibrium. However, with the non-Condon effect, the red side of the line is over pumped relative to the blue. Thus, there is a net flow of excited molecules from red to blue until the thermal equilibrium population distribution is obtained. The result is that there is a decrease in the excited state population on the

This article is copyrighted as indicated in the article. Reuse of AIP content is subject to the terms at: http://scitation.aip.org/termsconditions. Downloaded to IP: 171.64.123.74 On: Wed, 18 Mar 2015 16:17:11

red side of the line with the spectral diffusion time constants, and there is the corresponding increase in the excited state population on the blue side of the line. The red-blue difference can be seen clearly in the inset in Figure 4 by comparing the black and red curves.

The result on the PP observable is that components of the spectral diffusion faster than the vibrational lifetime will appear as decays and growths in the PP waiting time traces. If the population relaxation was slower than all of the spectral diffusion timescales, then all of them would be visible in the isotropic PP decays. For the present experiments, the slowest spectral diffusion dynamics are on the same timescale as (water), or slower than (methanol and ethanol), the vibrational lifetimes (Table II and Figure 5). Therefore, only the first two timescales of spectral diffusion appear as fast multiexponential components in the pump-probe decays. This relaxation of a nonequilibrium excited state population distribution toward the equilibrium population of absorbers via spectral diffusion is analogous to a transient hole burning experiment.[38,49] The final isotropic PP 0-1 transition decay has positive amplitude at all frequencies. The amplitude tracks the shape of the linear absorption spectrum and the decay corresponds to true population relaxation. These population decay times (lifetimes) are presented in Figure 5 as a function of detection frequency.

Examination of the vibrational lifetimes displayed in Figure 5 shows a trend towards faster population relaxation as the frequency moves to the red, which corresponds to the detection of O–D groups engaged in stronger hydrogen bonds. Vibrational lifetimes with a very strong frequency dependence can be an indicator that (at least) two distinct subensembles of molecules with different lifetimes are contributing to the isotropic PP decay. As discussed above, two subensembles that have different lifetimes would display biexponential decays with the amplitudes of the two decay components varying with frequency. However, the frequency dependence of the vibrational lifetimes in Figure 5 is very mild; this is in part a result of the fast spectral diffusion causing molecules to sample a significant fraction, but not all, of the inhomogeneous line prior to vibrational relaxation. Population relaxation requires accepting modes, internal and external, to take up the initial vibrational excitation energy. The rate of relaxation depends on the strength of the coupling to the accepting modes and their density of states.[50] Both of these can vary with wavelength. A red shift in frequency is associated with stronger hydrogen bonding, which can provide stronger coupling to accepting modes.

Therefore, we conclude that the hydroxyl stretch bands for water, methanol, and ethanol in $EmimNTf_2$ consist of single inhomogeneous distributions of local environments. Water (HOD) has the longest lifetime of the probes considered: between 19 and 22 ps. We find a much longer lifetime than for HOD in bulk water (1.7 ps[46,47]), likely due to the weak coupling to the surroundings. The lifetime shortens upon increasing the carbon chain length by one for methanol-d_4, with time constants between 11.6 and 12.2 ps. Methanol-OD (CH_3OD) displayed an even shorter lifetime of about 8 ps (not shown). Additional intramolecular modes, particularly C–H bends or stretches, can greatly reduce the deuteroxyl lifetime from the value for water. Ethanol-d_6 was found to have similar but slightly longer lifetimes than perdeuterated methanol: between 12.2 and 13.6 ps. The OD stretch is likely most strongly coupled to the modes associated with the carbon it is directly bonded to. In going from methanol to ethanol, the methyl becomes a methylene, with fewer high frequency modes, which may account for the small lengthening of the OD lifetime for ethanol-d_6.

The non-Condon effects and the shorting of the vibrational lifetime as the observed frequency is shifted to the red for water, methanol, and ethanol in the RTIL shows that the interaction of hydroxyls with their ionic environments has the characteristics of a hydrogen bond. The hydroxyls, which are hydrogen bond donors, presumably interact preferentially with the NTf_2^- anions. The red shift of the absorptions (see Figure 1) relative to the OD stretch of HOD in H_2O (2509 cm^{-1}) shows that the hydrogen bonding in the RTIL is much weaker than in water. Although weaker, the hydroxyl-RTIL interaction has the observable characteristics of the hydroxyl acting as a hydrogen bond donor.

VI. ORIENTATIONAL RELAXATION

The orientational relaxation dynamics can also be obtained from the polarization selective IR pump-probe experiments. The orientational anisotropy is given by

$$r(t) = \frac{2}{5}C_2(t) = \frac{I_{||}(t) - I_{\perp}(t)}{I_{||}(t) + 2I_{\perp}(t)}, \tag{4}$$

where $C_2(t)$ is the second Legendre polynomial orientational correlation function of the transition dipole moment (taken to be parallel to the O–D bond vector[37]). The anisotropy begins from a value of 0.4 at $t = 0$, corresponding to complete orientational correlation, and in the long-time, limit decays to zero for isotropic liquid samples. We ordinarily consider the isotropic signal denominator to divide out population decay dynamics, but in fact, it removes all isotropic dynamics, including the fast spectral diffusion components discussed in Sec. V.

The anisotropy decays were determined for water, methanol, and ethanol within the same range of frequencies for which the isotropic signal decays were examined in Sec. V. Examples of the methanol anisotropy decay data (symbols) are shown in Figure 6 for several of the frequencies that were studied. The data for water and ethanol have very similar appearances. The maximum observable time for water was about twice that accessible for the alcohols because of the relatively long vibrational lifetime of HOD (Figure 5).

As can be seen in Figure 6 and is also the case for all of the data for the three solutes, at $t = 0$ (extrapolation of the data from 280 fs to 0), the value of the anisotropy is significantly below 0.4. In Figure 6, the initial values vary from ~0.27 to ~0.33 depending on the frequency. For all of the solutes, the variation is between 0.25 and 0.33 across frequencies. The drop from 0.4 is due to an extremely fast sampling of orientational space by the inertial motions of the vibrational probe during and immediately following excitation by the pump pulse.[51,52] This essentially ballistic motion of the

This article is copyrighted as indicated in the article. Reuse of AIP content is subject to the terms at: http://scitation.aip.org/termsconditions. Downloaded to IP: 171.64.123.74 On: Wed, 18 Mar 2015 16:17:11

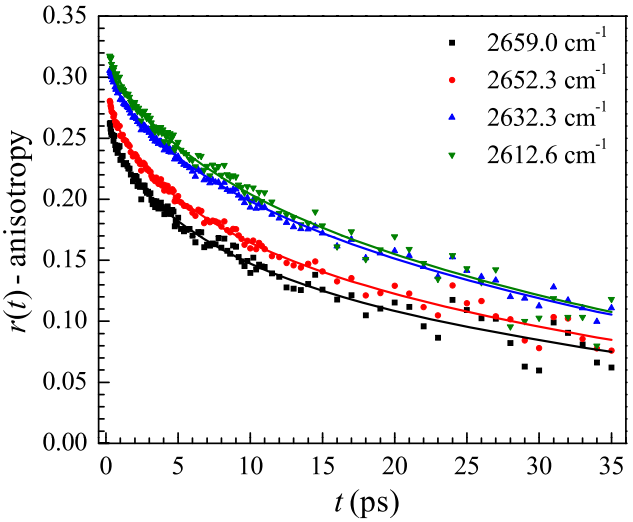

FIG. 6. Anisotropy decay data (symbols) for methanol-d_4 in $EmimNTf_2$ at several representative wavelengths. Solid lines are simultaneous tri-exponential fits to all frequencies. Data and fits for the other samples have very similar appearances.

solute is complete well within the first couple 100 fs after the pump.[51,52] There is a marked frequency dependence to the magnitude of this inertial motion.[51] The lower frequency data (top curve in Figure 6) have the largest initial anisotropy. In contrast, the higher frequency data have a large initial drop from 0.4. The degree of inertial orientational motion exhibited by the probes at various frequencies can be related to the shape of the angular potential in which they are reorienting. A complete analysis of this potential, using the harmonic cone model introduced by Moilanen *et al.*,[51] will be taken up later in this section.

For the simplest model of orientational relaxation, free diffusion, the orientational correlation function (following the ultrafast inertial motion) is proportional to $\exp(-6Dt)$, where D is the orientational diffusion constant. The anisotropy decay curves for water, methanol, and ethanol, however, are not single exponentials. Data for water are fit well with a biexponential decay function at each detected wavelength. The anisotropy decays for methanol and ethanol require a triexponential function to obtain high quality fits. Examples of the fits for methanol are the solid curves in Figure 6. For all wavelengths and all three samples, the fits are of same quality as those shown in Figure 6. All of the fits to the anisotropy curves decay to zero. In each case, the multiexponential fits with time constants t_1 through t_3 were determined for all frequencies simultaneously; the values are given in Table III. Determining the time constants through independent fits at single wavelengths did not result in a better description of the experimental curves. The corresponding amplitudes A_1 through A_3 (see supplementary material, Table SI[29] for values) were allowed to vary independently. In all cases, the fits are in quantitative agreement with the experimental anisotropy data.

In Sec. V, we showed that the multi-exponential isotropic PP decays were caused by spectral diffusion at short time, with a final single slowest exponential being the vibrational lifetime decay. For each solute, the data show that a single ensemble underlies the inhomogeneously broadened absorption line. Therefore, the multi-exponential orientational anisotropy decays are not caused by multiple subensembles having distinct orientational relaxation behavior. A well-developed and widely applicable framework that accounts for single ensemble multiple exponential decays of the orientational correlation function is the wobbling-in-a-cone model.[53–56] In this model, the molecule and its associated transition dipole is assumed to undergo orientational diffusion in angular space within a cone of half angle θ_0; configurations with the polar angle $\theta > \theta_0$ are not sampled. Therefore, only a limited range of angles are sampled, which does not cause the anisotropy to decay to zero. If this motion is followed by a slower process that completely randomizes orientations (anisotropy decays to zero), the resulting orientational correlation function is a biexponential decay. As discussed in the supplementary material,[29] the plateau to which the correlation function would decay in the absence of this final angular motion gives Q^2, the square of a generalized order parameter. From this plateau, the cone half angle θ_0 can be found according to[53]

$$Q^2 = \left(\frac{1}{2}\cos\theta_0\,(1+\cos\theta_0)\right)^2. \tag{5}$$

Previously, the wobbling-in-a-cone model was extended to treat the relevant case of an ultrafast inertial motion preceding restricted angular diffusion.[57] This form of the orientational correlation function (Eq. (S3) in the supplementary material[29]) is sufficient to describe the biexponential anisotropy decays found for water in the RTIL.

To address the triexponential decays observed with the probes methanol and ethanol, an extension of the model is required. The new wobbling-in-a-cone model for the orientational correlation function includes three distinct timescales of restricted angular diffusion following the ultrafast inertial orientational relaxation. After two wobbling components, the slowest decay is the complete reorientation of the solute. The form describing the total observed decay is given by

TABLE III. Time constants from biexponential (water) and triexponential (methanol and ethanol) fits to the anisotropy decay. The time scales τ_{c1}, τ_{c2}, τ_m, and D_m^{-1} are from the wobbling-in-a-cone analysis of the orientational correlation function (see text).

Vibrational probe	$t_1 = \tau_{c1}$ (ps)	t_2 (ps)	τ_{c2} (ps)	$t_3 = \tau_m$ (ps)	D_m^{-1} (ps)
HOD	...	4.0 ± 0.5	4.7 ± 0.7	25.1 ± 0.7	151 ± 4
Methanol-d_4	0.8 ± 0.1	5.6 ± 0.7	6.4 ± 0.9	42 ± 1	254 ± 8
Ethanol-d_6	0.8 ± 0.1	9.2 ± 0.9	10 ± 1	88 ± 10	530 ± 61

This article is copyrighted as indicated in the article. Reuse of AIP content is subject to the terms at: http://scitation.aip.org/termsconditions. Downloaded to IP: 171.64.123.74 On: Wed, 18 Mar 2015 16:17:11

$$C_2(t) = (1 - T^2)\exp(-t/\tau_{in}) + T^2(1 - S^2)\exp(-t/\tau_{c1}) + T^2S^2(1 - R^2)\exp(-t(1/\tau_{c2} + 1/\tau_m)) + T^2S^2R^2\exp(-t/\tau_m). \quad (6)$$

Here, T, S, and R are generalized order parameters describing the three cones which each extend the range of restricted motion of the transition dipole in turn. The correlation timescales are τ_{in}, τ_{c1} and τ_{c2}, with the subscripts in, c_1 and c_2 for the inertial cone, the first diffusive cone and the second diffusive cone, respectively. The final timescale of free diffusion, which causes complete orientational randomization, is τ_m. Since the inertial motion in the first term (time scale τ_{in}) is complete before the observable time evolution of $C_2(t)$ begins, Eq. (6) describes a triexponential decay of the data. Equation (6) is derived in the supplementary material[29] following the method of Tan *et al.*[57] The biexponential case (Eq. (S3) in the supplementary material[29]) is recovered if there is no motion on the timescale of τ_{c1}, that is, $S = 1$. We use the notation in Eq. (6) for both the two-cone (water) and three-cone (methanol and ethanol) cases.

The interpretation of an orientational correlation function incorporating several cones is straightforward. Any diffusive angular motion must proceed by fast, limited ballistic angular steps, so the inertial cone angle is a general feature of these orientational correlation functions at exceedingly short times (<100 fs). The diffusive motion of the solute on longer timescales can be limited by constraints imposed by the environment, which changes slowly on the timescale of angular diffusion. As the timescale is increased even further, environmental fluctuations lead to a relaxation of these constraints and further diffusion can occur. In complex liquids like the RTIL studied here, there may be multiple timescales on which the angular space accessible to the probe is limited. Each restricted cone correlation function in $C_2(t)$ represents a constraint to free diffusion that is relaxed following the wobbling timescale.

It is straightforward using Eq. (6) to extract the generalized order parameters for each of the three cones and the total order parameter $Q = TSR$, along with the correlation times $\tau_{c1} = t_1$, $\tau_{c2} = (1/t_2 - 1/t_3)^{-1}$, and $\tau_m = t_3$, from a general triexponential fit to experimental anisotropy data. Because the final decay of the orientational correlation function is by free diffusion, the diffusion constant for this process is given by[53]

$$D_m = \frac{1}{6\tau_m}. \quad (7)$$

Table III gives the second wobbling correlation time τ_{c2} and long time free diffusion timescale D_m^{-1} for each vibrational probe as determined within the wobbling-in-a-cone model. The diffusion constants for periods of restricted angular motion are generally functions of both the anisotropy decay time constant and the cone half angle. For a wobbling motion described by a cone of semiangle θ_0 and order parameter Q, with $x = \cos\theta_0$ and time constant for wobbling τ_c, then the diffusion constant is given by[53]

$$D_c = \frac{x^2(1 + x)^2[\ln((1 + x)/2) + (1 - x)/2]}{\tau_c(1 - Q^2)(2(x - 1))} + \frac{(1 - x)(6 + 8x - x^2 - 12x^3 - 7x^4)}{24\tau_c(1 - Q^2)}. \quad (8)$$

Results of the complete wobbling-in-a-cone analysis for the solutes water, methanol, and ethanol at all wavelengths studied are given in Figure 7 and in the supplementary material, Table SII.[29] The diffusion constant D_{c1} is associated with the timescale τ_{c1} and cone angle θ_{c1}, determined from S. Likewise, D_{c2} corresponds to τ_{c2}, θ_{c2}, and R. In Table III and Table SII in the supplementary material,[29] we show inverse diffusion constants, that is, the diffusion timescales, for easier comparison to other time constants. There is no time constant for the inertial cone, characterized by angle θ_{in} and order parameter T, because we only know this motion is faster than can be observed experimentally. The total wobbling cone half angle θ_{tot} is due to the total order parameter Q; this cone characterizes the full range of angular space which is sampled in all the periods of restricted orientational diffusion (or inertial motion) taken together.

The frequency-dependent cone angles are compared for water, methanol, and ethanol in Figure 7. Note that there is a single frequency axis but the line centers for the three solutes are not the same (see Figure 1). So, points for different samples at the same frequency are at different positions relative to their respective absorption maxima. The data points for HOD in Figure 7 and Tables SI and SII in the supplementary material[29] do not extend as far to the red as those for methanol and ethanol because both the 1-2 transition and the spectrum of D_2O cause interference in the PP data in this spectral region. All of the inertial cone angles and their wavelength dependences are almost identical for the three solutes. Therefore, the hydroxyls sample virtually the same range of angular space through the inertial motion. Furthermore, as the wavelength shifts to the red, which is associated with stronger hydrogen bonding, the inertial cone gets smaller. As discussed further below, this is consistent with the behavior of HOD in water.[51] In terms of the potential surface on which the inertial motion occurs, the stronger hydrogen bond produces a steeper potential that limits the range of angular inertial motion.

The hard cone potential [53–56] in the wobbling-in-a-cone analysis is a useful model but not fully physically realistic, particularly for the ultrafast inertial motion. Rather than experiencing free diffusion before encountering a hard wall, a better approximation for the restricted reorientation involves angular motion within a harmonic potential, as introduced by Moilanen *et al.*[51] For a center position of $\theta = 0$, the harmonic potential induces a Gaussian distribution of probability for the polar angle, which is independent of the azimuthal angle. In the harmonic cone model, the angular probability distribution is given by[51]

$$p(\theta) = \exp\left(-\frac{\theta^2}{2\theta_H^2}\right), \quad (9)$$

with the harmonic cone angle

$$\theta_H^2 = \frac{kT}{I\omega^2}. \quad (10)$$

Here, I is the moment of inertia and ω is the angular frequency characterizing the curvature of the harmonic potential.[51,58] As pointed out by Ramasesha *et al.*,[58] for reasonably small hard cone angles θ_0 (we find $\theta_0 \leq 30°$ gives negligible error), there is an excellent approximation $2\theta_H = \theta_0$. The inertial cone

This article is copyrighted as indicated in the article. Reuse of AIP content is subject to the terms at: http://scitation.aip.org/termsconditions. Downloaded to IP: 171.64.123.74 On: Wed, 18 Mar 2015 16:17:11

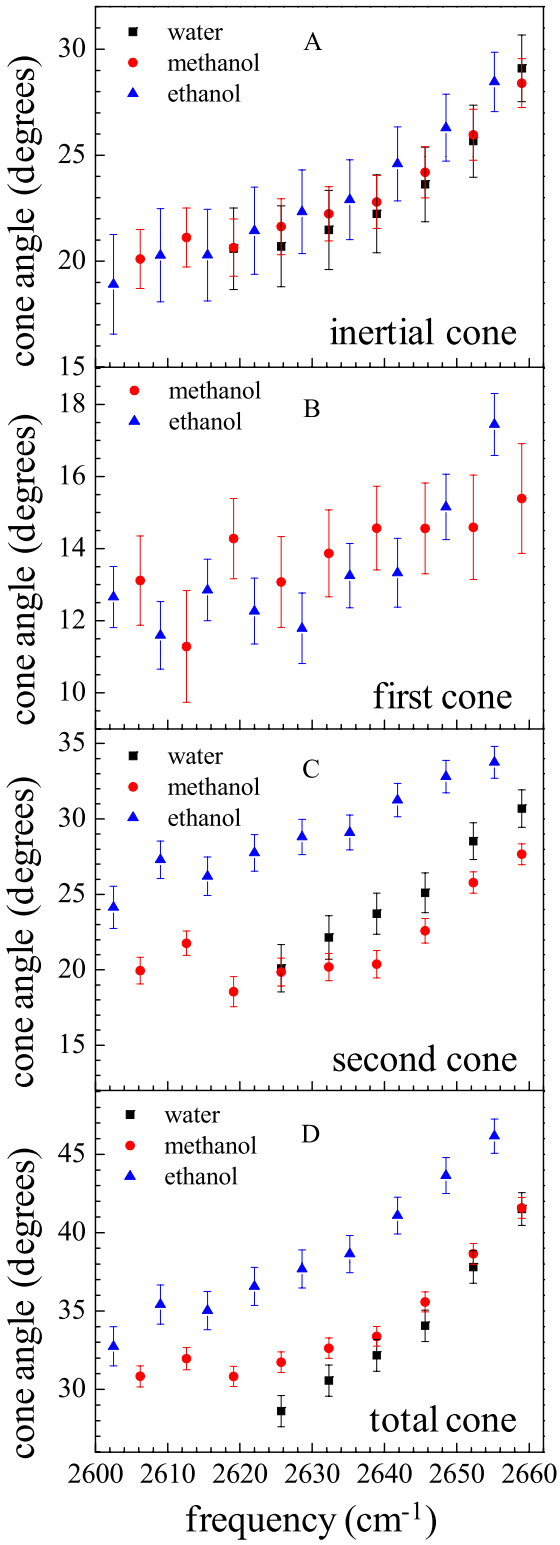

FIG. 7. Cone half angles as a function of frequency for HOD, methanol-d_4, and ethanol-d_6 as a function of wavelength. (a) Inertial cone. (b) First wobbling cone. (c) Second wobbling cone. (d) Total cone. Water exhibits only one period of restricted orientational diffusion following the inertial motion so the first cone is not present.

angles reported in Figure 7 and Table SII[29] using the hard cone model can be directly related to an equivalent harmonic cone angle, and hence the potential energy surface curvature. Knowledge of the moment of inertia then allows calculation of the frequency ω of the harmonic potential according to Eq. (10).

However, there is some ambiguity in the choice of value for the moment of inertia. In the study of water (HOD in H_2O), the average of the three principal moment of inertia components determined for rotation about the center of mass was used.[51] This is a reasonable approximation for water where the center of mass is almost on the oxygen atom, and it probably makes sense that the orientational motion occurs around or close to around the center of mass. For methanol and ethanol, it is not clear that the angular motion will occur about the center of mass. For example, depending on the structure of the local environment, ethanol might undergo angular excursions about the center of the methyl group. Therefore, we will focus on water (HOD), which permits a comparison to bulk water.[51] Similar qualitative conclusions should hold for the angular potentials of methanol and ethanol even if the frequencies cannot be directly calculated using (10).

Using Eq. (10) and the cone angles given in Figure 7(a) and Table SII in the supplementary material,[29] the observation frequency dependent harmonic potential frequencies can be obtained as was done for HOD in water.[51] For HOD, the average moment of inertia, that is, the average of the three principal components is $I = 2.849 \times 10^{-47}$ kg · m^2.[51,59] Figure 8 shows a plot of the HOD harmonic potential frequencies in the RTIL (black squares) and those for HOD in H_2O vs. the pump-probe detection frequency (red circles). The HOD in H_2O spectrum is much broader than the HOD in RTIL spectrum. The HOD in H_2O data spans the frequency range from the far blue side of the line to just past the center frequency (2509 cm^{-1}), while the HOD in RTIL data goes from the blue side of the line to somewhat past the center frequency (2646 cm^{-1}). For both samples, as the frequency moves from blue to red, the harmonic potential frequency increases; that is, the potential surface on which the angular motion is occurring becomes steeper. A red shift in absorption is generally interpreted as reflecting a stronger hydrogen bond.[13,20–22] So, the increase in the harmonic potential frequency with decreasing experimental frequency may be associated with stronger

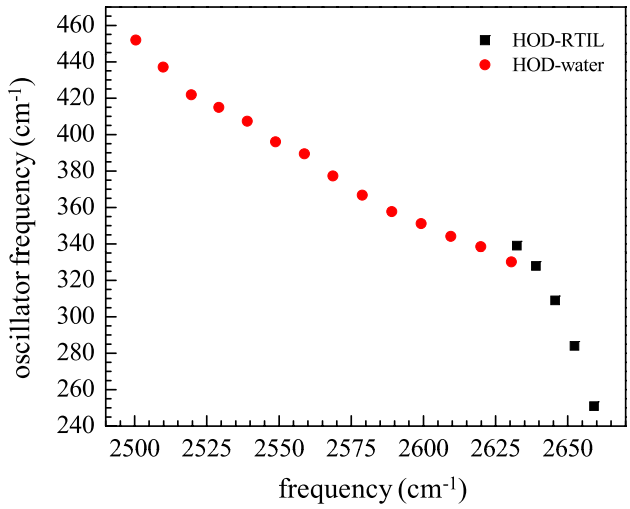

FIG. 8. Oscillator frequencies reflecting the harmonic potential associated with the inertial motion of HOD in $EmimNTf_2$ (black squares) and in bulk water[51] (red circles).

This article is copyrighted as indicated in the article. Reuse of AIP content is subject to the terms at: http://scitation.aip.org/termsconditions. Downloaded to IP: 171.64.123.74 On: Wed, 18 Mar 2015 16:17:11

hydrogen bonding inhibiting the inertial angular motion. Figure 8 shows that the highest harmonic potential frequency for HOD in the RTIL, which occurs on the red side of the absorption spectrum, is about the same as the lowest harmonic potential frequency for HOD in H_2O, which occurs on the blue side of its spectrum. This result is consistent with the blue shift of the absorption spectrum of HOD in the RTIL relative to HOD in water being associated with weaker hydrogen bonding.

The change in the harmonic potential frequency vs. experimental frequency of HOD in the RTIL is much steeper than that of HOD in H_2O. However, the HOD in H_2O absorption band is much broader (170 cm^{-1}) than that of HOD in the RTIL (45 cm^{-1}). The HOD in H_2O data (Figure 8, red circles) can be fit with a line that has slope of −0.9. The HOD in the RTIL data (Figure 8, black squares) changes more gradually past the line's center frequency than it does on the blue side. If only the four highest frequency points are fit, which go from the blue side of the absorption spectrum to past line center, the slope is −3.8. The ratio of the slopes is virtually the same as the ratio of the linewidths. So, the change in the harmonic potential frequency relative to the change in the detection frequency as a fraction of the line width is virtually the same for the two samples. These results show that a change in the hydrogen bond strength produces less change in the absorption frequency for HOD in the RTIL than it does for HOD in H_2O.

As mentioned above, after the initial inertial drop from $r(t) = 0.4$, the water anisotropy data are fit well by a bi-exponential function. The HOD molecules undergo a restricted wobbling motion followed by complete orientational relaxation. The methanol and ethanol data require a tri-exponential to obtain a good fit. Therefore, the alcohols undergo two distinct wobbling motions followed by the complete orientational randomization. The time constants associated with the wobbling motions and the final complete orientational randomization are give in Table III. The cone angles for all of the cones (inertial, first cone, second cone) as well as the total cone angle, which is the total half angle sampled by the restricted motions prior to complete randomization, are shown in Figure 7 and the values are given in the supplementary material, Table SII.[29]

Although the experiments are conducted on the O–D stretch of HOD, both hydroxyls of HOD are capable of forming hydrogen bonds with anions.[10] Water may lack the first fast wobbling component (first cone) because it makes two hydrogen bonds, while the alcohols form only one. In contrast to water, both alcohols display a very fast component of the anisotropy decay with time constants of 0.8 ± 0.1 ps. As shown in Figure 7(b), the cone angles and the frequency dependence of the cone angles for methanol and ethanol are the same within experimental error. Compared to the inertial and the second cone, the first cone angles are relatively small and show a small change in angle with frequency. The very weak frequency dependence may suggest that the hydrogen bond angular potential is of less importance to this motion than the earlier inertial motion and later, larger scale, diffusive wobbling.

All three solutes exhibit restricted diffusive motion with correlation times, τ_{c2}, in the range 5–10 ps for the second cone (see Table III). While water and methanol sample a similar range of 15°–30° in 5-6 ps, ethanol wobbles in a larger cone of about 25°–35° (see Figure 7(c)) and has a longer correlation time of 10 picoseconds. Because of ethanol's larger wobbling second cone angle, its total cone of angles sampled before free diffusion is the largest of the group. Water and methanol have rather similar total cone angles at all wavelengths (Figure 7(d)). In all the samples, the slopes of the cone angles versus frequency are very similar, indicating that the rate of change of hydrogen bond strengths with frequency are generally equivalent among water, methanol, and ethanol. Unlike the first cone, which is present for only the alcohols, this wobbling motion likely involves significant configurational changes of the hydrogen bond.

The complete orientational randomization time, τ_m, is where the size of the solutes has a major influence. Table III shows that the orientational correlation times for water, methanol, and ethanol are 25 ps, 42 ps, and 88 ps, respectively. Reorientation slows dramatically with increasing solute size. Qualitatively, the orientational relaxation times progress as expected, that is, the larger the solute the longer the relaxation time. Because the bulk viscosity is unaffected by the very low solute concentrations, the increase in orientation relaxation time with size could be simple hydrodynamics.

We can compare the trend in relaxation times to that predicted by hydrodynamics using a modified Debye-Stokes-Einstein (DSE) equation[60–62]

$$\tau_m = \frac{f V_{\text{eff}} \eta}{k_B T}, \tag{11}$$

where $f = 1$ for the stick boundary condition. The temperature T and the viscosity, η, are constant. Therefore, the scaling of reorientation times is determined by the product $f V_{\text{eff}}$. Because the solutes are much smaller than the RTIL ions, the stick boundary condition, in which the solvent surrounding a solute rotates along with it, is unlikely to hold. Taking the volumes of water, methanol, and ethanol to be approximately 10.3, 31.5, and 48.7 $Å^3$, respectively, we obtain normalized ratios τ_m/V_{eff} of 1.0, 0.55, and 0.74, where the ratio for water is normalized to 1. That the ratio is not constant shows that hydrodynamics with the stick boundary condition does not describe the orientational relaxation. Alternatively, for slip boundary conditions, which occur when the solute is much smaller than the solvent molecules, there is no fluid velocity component transverse to the solute surface. The friction is entirely due to displacement of solvent molecules when the solute rotates. This effect enters Eq. (11) through f, which is a function of the rotating molecule's shape. For a solute modeled as a spheroid (either prolate or oblate), we write $f = f(\rho)$, where ρ is the ratio of minimum to maximum semiaxes lengths; the values of $f(\rho)$ have been tabulated.[62] We model water as an oblate spheroid with $\rho \approx 0.80$ and methanol and ethanol as prolate spheroids with approximate ρ values of 0.80 and 0.65, respectively. The normalized ratios $\tau_m/(f(\rho)V_{\text{eff}})$ are 1.0, 0.56, and 0.22, again relative to the value for water. If hydrodynamic orientational relaxation occurred with slip boundary conditions, the three values would all be 1. The large discrepancy in these values, which display a significant downward trend, demonstrates that the slip

This article is copyrighted as indicated in the article. Reuse of AIP content is subject to the terms at: http://scitation.aip.org/termsconditions. Downloaded to IP: 171.64.123.74 On: Wed, 18 Mar 2015 16:17:11

boundary conditions are not applicable for rotation in these systems.

Two forms of the DSE equation, with the stick and slip boundary conditions, fail to adequately describe the trend in reorientation times as the solute is changed from water to ethanol. The trend in the solute orientational relaxation is not described well with a simple hydrodynamic model. This is not surprising. All three solutes should hydrogen bond to anions. The three solutes reside in highly complex environments with specific intermolecular interactions with the surrounding ions. The solutes not only have different sizes but will also have distinct local interactions. The nature of the solute will impact the specific hydrogen bond interactions as well as the ion fluctuations necessary for total reorientation. It should be noted that the non-hydrodynamic behavior is in contrast to the hydrodynamic behavior displayed by large solutes in RTILs.[63,64]

VII. HYDROGEN BONDING IN AN RTIL: SPECTRAL AND ORIENTATIONAL FLUCTUATIONS

Through 2D IR measurements of spectral diffusion (Sec. IV) and polarization selective pump-probe measurements of orientational relaxation (Sec. VI), we have characterized a complex series of fluctuations of the hydrogen-bonded hydroxyl (O–D) group on solutes in the RTIL $EmimNTf_2$. These two independent and complementary observables show hydroxyl motions on roughly corresponding timescales of a few hundred femtoseconds, several picoseconds, and several tens of picoseconds (Tables II, III, and in Table SII in the supplementary material[29]). Additionally, the FFCF extracted from the experimental CLS shows a significant homogenous contribution to the line shape, caused by fluctuations on ultrafast timescales, typically <100 fs. Similarly, all of the solutes (water, methanol, and ethanol) exhibit an ultrafast inertial orientational relaxation component that is complete in <200 fs.

Because the FFCF and anisotropy are different correlation functions, the timescales of their respective decays are not necessarily directly comparable. However, the striking similarity between their functional forms, and even the time constants, is suggestive that to at least some extent, the same underlying motions of the solutes, solvating ions, or both are simultaneously causing both the orientational relaxation and spectral diffusion dynamics. Situations in which orientational and spectral coordinates are coupled are starting to receive some attention.[58] An example is HOD in bulk water. Large-angle jump reorientation causes the decay of the orientational correlation function.[65,66] Similarly, the slowest decay of the frequency-frequency correlation function is caused by rearrangements of the hydrogen bond network,[21,22] with hydrogen bond switching occurring primarily by the same angular jumps that cause the anisotropy to decay. However, the slowest component of the spectral diffusion, 1.7 ps,[20,43] is not identical to the anisotropy decay, 2.6 ps.[51] The network rearrangements that give rise to spectral diffusion by changing the strength of a particular O–D oscillator's hydrogen bond interactions can occur without the O–D itself moving; its neighbors are equally likely to undergo large angle jumps.

In the RTIL-hydroxyl systems examined in the present work, the situation is quite different. As discussed in Secs. II B and III, essentially all of the hydroxyls observed by our infrared experiments are hydrogen bonded to anions; they are spatially isolated from other hydroxyl-bearing probe molecules. Therefore, a change in hydrogen bonding configuration must involve either a motion of the *observed* hydroxyl (O–D) group or the solvating ions. Optical Kerr effect studies have shown that the timescales of total rearrangement of the ions in water-RTIL mixtures, with similarly large ion pair to water ratio as the samples studied here, are approximately one nanosecond,[67] far slower than the timescales of spectral diffusion and orientational relaxation we have observed. Hydrogen bond evolution driven by large scale reorientation of solvating molecules is thus unlikely to be the major contributor to the FFCF decays. However, without complete randomization of the RTIL structure, which includes rearrangements of the alkyl tails, the ions can still undergo local structural changes. Hydrogen bond length fluctuations caused by the water/alcohol solute and/or ion translations and orientational motions can be key contributors to spectral diffusion[25] that occurs on a time scale faster than complete orientational randomization of the RTIL.

Terranova and Corcelli[25] found that the major contributor to the MD simulated FFCF decay of dilute water in a similar RTIL[24] was anion translational motions. These MD simulations indicated that rotational motions of the constituent ions correlated to a much lesser extent with the spectral diffusion.[67] This decomposition, however, does not address the influence of the vibrational probe reorienting relative to its surrounding ion solvation shell. Rotation of the O–D group when viewed from the frame of the hydroxyl can have significant anion translational contributions. The short time components of the spectral diffusion for water, methanol, and ethanol are 0.5 ± 0.1 ps, 0.3 ± 0.1 ps, and 0.4 ± 0.1 ps, respectively. The intermediate time components for the three solute molecules are 5 ± 1 ps, 3.4 ± 0.8 ps, and 4.2 ± 0.7 ps. Therefore, within experimental error, the short time components and intermediate time components are the same for the three solutes. These results indicate that these dynamics are independent of the size of the solute. It is reasonable then to assign the first two timescales of spectral diffusion to the same types of fluctuations for the three solutes. For HOD in bulk water, the fastest component of the spectral diffusion is 0.4 ps.[20,43] MD simulations show that this fast component is caused principally by very local hydrogen bond length fluctuations.[20,43] Given that the fastest component of the spectral diffusion observed here for all three solutes is the same as that observed for HOD in bulk water within experimental error, it is likely that this component is also caused by hydrogen bond length fluctuations.

While the time scale for orientational randomization of the entire RTIL is very long, the cations and anions can also undergo restricted orientational relaxation (wobbling), which will contribute to spectral diffusion. It is also possible that orientational motions of the solutes themselves contribute to the fast and intermediate time scale spectral diffusion. However, water does not have an observable fast wobbling motion (first cone) and the wobbling dynamics of the second

This article is copyrighted as indicated in the article. Reuse of AIP content is subject to the terms at: http://scitation.aip.org/termsconditions. Downloaded to IP: 171.64.123.74 On: Wed, 18 Mar 2015 16:17:11

cone are not the same for the three solutes. Table III gives the second cone wobbling time constants, τ_{c2}, but these cannot be compared directly because they have different cone angles. It is necessary to compare the inverse wobbling diffusion constants, D_{c2}^{-1}, which are obtained using Eq. (8) and are give in Table SII in the supplementary material.[29] Around the center of each absorption line, the values of D_{c2}^{-1} for water, methanol, and ethanol are ~80 ± 15 ps, ~165 ± 30 ps, and 150 ± 20 ps, respectively. While methanol and ethanol have the same inverse wobbling diffusion constants within experimental error, the wobbling motion of water is much faster. These results suggest that the wobbling motions of the solutes themselves are not major contributors to the fast and intermediate time spectral diffusion. Motions of the ions may not be strongly impacted by the presence of the relatively small solutes and the differences in the solute sizes will not have much influence on the fast motions of the ions. Such motions could account for the intermediate time component of the FFCF.

The longest timescale decays of the FFCFs (τ_3, Table II) and orientational correlation function (τ_m, Table III) show significant differences among the solutes. However, the differences in the spectral diffusion slowest decay time constants are much less than the differences in the slowest orientational relaxation time constants. In going from water to ethanol, spectral diffusion slows by a factor of ~1.5, while orientational relaxation slows by a factor of ~3.5. To fully reorient, the smaller water molecule is less likely to require large ion displacements than the larger alcohol probes. The difference between the solute size dependence for spectral diffusion and orientational relaxation suggests that large scale solute motion is not required for spectral diffusion. The increase in the slowest spectral diffusion time constant as the solute becomes larger may be caused by a screening of interactions between the hydroxyl and the RTIL by the alkyl groups. A common method used in MD simulations to couple the structural fluctuations of the system to the frequency of the vibration measured in a 2D IR experiments is to calculate the electric field fluctuations along the transition dipole of the vibration.[20,25,68] The fluctuating electric field is related to frequency fluctuations. This is the approach used in the recent simulation of HOD in a RTIL.[25] The methyl group of methanol and the ethyl group of ethanol will force a fraction of the ions to be more distant from the hydroxyls than they are for water, which would modify the nature of the electric field along the hydroxyl. Ion motions cause the electric field to fluctuate, but these ion motions can be influenced by the presence of the alkyl groups. The water/RTIL MD simulations indicate that ion translational motions are important in causing spectral diffusion.[25] The presence of the alkyl groups on the alcohols in the current study may slow the translation motion of a fraction of the ions giving rise to slower spectral diffusion.

VIII. CONCLUDING REMARKS

To elucidate the solute/RTIL dynamics, particularly those involving hydrogen bond fluctuations, we have presented 2D IR measurements of spectral diffusion and polarization selective pump-probe measurements of vibrational population dynamics and orientational relaxation for the hydroxyl stretch of water, methanol, and ethanol in $EmimNTf_2$. Analysis of the isotropic pump-probe signals demonstrated that the observed non-exponential dynamics had an early time contribution from spectral diffusion and the true population decay at longer times. From the frequency dependence of the population decay rates, a single component population of H-bonded hydroxyls was inferred for all three solutes. Non-Condon effects caused the pump pulse to create a nonequilibrium distribution of excited absorbers that relaxed toward the equilibrium distribution through the structural fluctuations that cause spectral diffusion. The manifestation of this time-evolving population in the isotropic PP decay is expected to be quite general for infrared resonances having a significant variation in the transition dipole moment with frequency.

The frequency-frequency correlation function, characterizing the structural evolution of the solute/RTIL systems (in particular the hydrogen bonding), and the orientational correlation function of the hydroxyl group both reported a variety of timescales for hydrogen bond strength fluctuation and orientational relaxation. These ranged between a few hundred femtoseconds and many tens of picoseconds. In addition to complete orientational randomization on the longest time scale, the solutes also underwent restricted angular diffusion in a range of cone angles. The cone angles and time dependences of the orientational motions were extracted from the pump-probe anisotropy decays. Spectral diffusion processes appeared on similar timescales to orientational relaxation but key differences in their respective trends between solutes suggest that ion translational (or ion hindered rotational) fluctuations play a larger role in spectral diffusion than solute reorientation. Experiments currently in progress will help clarify the coupling of spectral diffusion with orientational fluctuations for hydrogen bonded species in a RTIL. On the longest time scale, the spectral diffusion showed a substantially smaller change in dynamics with increasing solute size than the orientational relaxation. While orientational relaxation requires large scale motion of the solute molecules, spectral diffusion does not. Complete spectral diffusion can be caused by the structural evolution of the RTIL without large scale translation or rotation of the solute.

Understanding the dynamics of small but ubiquitous molecules such as water and alcohols in ionic liquids may prove useful for the design of RTIL-solute and RTIL-cosolvent systems tailored to various purposes. Additionally, the development of simulation tools and methodology for treating both the ionic liquid and the vibrational probes will benefit from comparison to the measurements presented here.

ACKNOWLEDGMENTS

We thank Jun Nishida, Amr Tamimi, and Christian Lawler for many stimulating discussions. This work was funded by the Division of Chemical Sciences, Geosciences, and Biosciences, Office of Basic Energy Sciences of the U.S. Department of Energy through Grant No. DE-FG03-84ER13251. P.L.K. acknowledges an Abbott Laboratories Stanford Graduate Fellowship.

This article is copyrighted as indicated in the article. Reuse of AIP content is subject to the terms at: http://scitation.aip.org/termsconditions. Downloaded to IP: 171.64.123.74 On: Wed, 18 Mar 2015 16:17:11

[1]N. V. Plechkova and K. R. Seddon, Chem. Soc. Rev. **37**, 123-150 (2008).
[2]T. Welton, Chem. Rev. **99**(8), 2071-2084 (1999).
[3]J. P. Hallett and T. Welton, Chem. Rev. **111**(5), 3508-3576 (2011).
[4]A. Pinkert, K. N. Marsh, S. Pang, and M. P. Staiger, Chem. Rev. **109**(12), 6712-6728 (2009).
[5]Y. Kohno and H. Ohno, Chem. Commun. **48**(57), 7119-7130 (2012).
[6]K. Fujita, D. R. MacFarlane, and M. Forsyth, Chem. Commun. **2005**(38), 4804-4806.
[7]K. Fujita, M. Forsyth, D. R. MacFarlane, R. W. Reid, and G. D. Elliott, Biotechnol. Bioeng. **94**, 1209-1213 (2006).
[8]E. W. Castner, C. J. Margulis, M. Maroncelli, and J. F. Wishart, Annu. Rev. Phys. Chem. **62**(1), 85-105 (2011).
[9]M. Armand, F. Endres, D. R. MacFarlane, H. Ohno, and B. Scrosati, Nat. Mater. **8**(8), 621-629 (2009).
[10]L. Cammarata, S. G. Kazarian, P. A. Salter, and T. Welton, Phys. Chem. Chem. Phys. **3**, 5192-5200 (2001).
[11]A. Mele, C. D. Tran, and S. H. De Paoli Lacerda, Angew. Chem., Int. Ed. **42**(36), 4364-4366 (2003).
[12]R. Hayes, S. Imberti, G. G. Warr, and R. Atkin, Angew. Chem., Int. Ed. **52**(17), 4623-4627 (2013).
[13]G. C. Pimentel and A. L. McClellan, *The Hydrogen Bond* (W. H. Freeman and Co., San Francisco, 1960).
[14]P. Ball, Chem. Rev. **108**(1), 74-108 (2008).
[15]C. D. Tran, S. H. De Paoli Lacerda, and D. Oliveira, Appl. Spectrosc. **57**, 152-157 (2003).
[16]E. T. J. Nibbering and T. Elsaesser, Chem. Rev. **104**, 1887-1914 (2004).
[17]H. J. Bakker and J. L. Skinner, Chem. Rev. **110**, 1498-1517 (2010).
[18]P. L. Geissler, Annu. Rev. Phys. Chem. **64**(1), 317-337 (2013).
[19]L. De Marco, M. Thämer, M. Reppert, and A. Tokmakoff, J. Chem. Phys. **141**(3), 034502 (2014).
[20]J. B. Asbury, T. Steinel, K. Kwak, S. A. Corcelli, C. P. Lawrence, J. L. Skinner, and M. D. Fayer, J. Chem. Phys. **121**, 12431 (2004).
[21]C. P. Lawrence and J. L. Skinner, J. Chem. Phys. **118**, 264-272 (2003).
[22]S. Corcelli, C. P. Lawrence, and J. L. Skinner, J. Chem. Phys. **120**, 8107-8117 (2004).
[23]C. Roth, A. Appelhagen, N. Jobst, and R. Ludwig, ChemPhysChem **13**, 1708-1717 (2012).
[24]D. B. Wong, C. H. Giammanco, E. E. Fenn, and M. D. Fayer, J. Phys. Chem. B **117**, 623-635 (2012).
[25]Z. L. Terranova and S. A. Corcelli, J. Phys. Chem. B **118**(28), 8264-8272 (2014).
[26]H. Shirota, T. Mandai, H. Fukazawa, and T. Kato, J. Chem. Eng. Data **56**(5), 2453-2459 (2011).
[27]O. Russina, A. Triolo, L. Gontrani, R. Caminiti, D. Xiao, L. G. Hines, R. A. Bartsch, E. L. Quitevis, N. V. Plechkova, and K. R. Seddon, J. Phys.: Condens. Matter **21**(42), 424121 (2009).
[28]K. Fujii, R. Kanzaki, T. Takamuku, Y. Kameda, S. Kohara, M. Kanakubo, M. Shibayama, S.-i. Ishiguro, and Y. Umebayashi, J. Chem. Phys. **135**(24), 244502 (2011).
[29]See supplementary material at http://dx.doi.org/10.1063/1.4914156 for the derivation of our wobbling-in-a-cone correlation function, anisotropy decay fit parameters, and additional wobbling-in-a-cone parameters.
[30]E. E. Fenn, D. B. Wong, and M. D. Fayer, J. Chem. Phys. **134**, 054512 (2011).
[31]H.-S. Tan, I. R. Piletic, and M. D. Fayer, J. Opt. Soc. Am. B **22**(9), 2009-2017 (2005).
[32]A. Tokmakoff, J. Chem. Phys. **105**(1), 1-12 (1996).
[33]S. Park, K. Kwak, and M. D. Fayer, Laser Phys. Lett. **4**, 704-718 (2007).
[34]P. Hamm and M. T. Zanni, *Concepts and Methods of 2D Infrared Spectroscopy* (Cambridge University Press, Cambridge, New York, 2011).
[35]K. Gaffney, I. R. Piletic, and M. D. Fayer, J. Phys. Chem. A **106**, 9428-9435 (2002).
[36]J. R. Schmidt, S. A. Corcelli, and J. L. Skinner, J. Chem. Phys. **123**, 044513 (2005).
[37]S. Corcelli and J. L. Skinner, J. Phys. Chem. A **109**, 6154-6165 (2005).
[38]S. Mukamel, *Principles of Nonlinear Optical Spectroscopy* (Oxford University Press, New York, 1995).
[39]F. W. Deeg and M. D. Fayer, J. Chem. Phys. **91**(4), 2269-2279 (1989).
[40]K. Kwak, S. Park, I. J. Finkelstein, and M. D. Fayer, J. Chem. Phys. **127**, 124503 (2007).
[41]S. M. G. Faeder and D. M. Jonas, J. Phys. Chem. A **103**(49), 10489-10505 (1999).
[42]K. Kwak, D. E. Rosenfeld, and M. D. Fayer, J. Chem. Phys. **128**(20), 204505 (2008).
[43]J. B. Asbury, T. Steinel, C. Stromberg, S. A. Corcelli, C. P. Lawrence, J. L. Skinner, and M. D. Fayer, J. Phys.Chem. A **108**, 1107-1119 (2004).
[44]D. E. Moilanen, D. Wong, D. E. Rosenfeld, E. E. Fenn, and M. D. Fayer, Proc. Natl. Acad. Sci. U. S. A. **106**(2), 375-380 (2009).
[45]M. Ji, M. Odelius, and K. J. Gaffney, Science **328**(5981), 1003-1005 (2010).
[46]T. Steinel, J. B. Asbury, J. R. Zheng, and M. D. Fayer, J. Phys. Chem. A **108**(50), 10957-10964 (2004).
[47]Y. L. A. Rezus and H. J. Bakker, J. Chem. Phys. **123**(11), 114502 (2005).
[48]R. Zwanzig, Annu. Rev. Phys. Chem. **16**(1), 67-102 (1965).
[49]I. R. Piletic, K. J. Gaffney, and M. D. Fayer, J. Chem. Phys. **119**, 423-434 (2003).
[50]V. M. Kenkre, A. Tokmakoff, and M. D. Fayer, J. Chem. Phys. **101**, 10618 (1994).
[51]D. E. Moilanen, E. E. Fenn, Y. S. Lin, J. L. Skinner, B. Bagchi, and M. D. Fayer, Proc. Natl. Acad. Sci. U. S. A. **105**(14), 5295-5300 (2008).
[52]J. J. Loparo, C. J. Fecko, J. D. Eaves, S. T. Roberts, and A. Tokmakoff, Phys. Rev. B **70**(18), 180201 (2004).
[53]G. Lipari and A. Szabo, Biophys. J. **30**(3), 489-506 (1980).
[54]G. Lipari and A. Szabo, J. Am. Chem. Soc. **104**(17), 4546-4559 (1982).
[55]C. C. Wang and R. Pecora, J. Chem. Phys. **72**(10), 5333-5340 (1980).
[56]K. Kinosita, S. Kawato, and A. Ikegami, Biophys. J. **20**, 289-305 (1977).
[57]H.-S. Tan, I. R. Piletic, and M. D. Fayer, J. Chem. Phys. **122**, 174501 (2005).
[58]K. Ramasesha, S. T. Roberts, R. A. Nicodemus, A. Mandal, and A. Tokmakoff, J. Chem. Phys. **135**(5), 054509 (2011).
[59]D. Eisenberg and W. Kauzmann, *The Structure and Properties of Water* (Oxford University Press, 2005).
[60]R. S. Moog, M. D. Ediger, S. G. Boxer, and M. D. Fayer, J. Phys. Chem. **86**, 4694-4700 (1982).
[61]G. K. Youngren and A. Acrivos, J. Chem. Phys. **63**, 3846-3849 (1975).
[62]C.-M. Hu and R. Zwanzig, J. Chem. Phys. **60**, 4354-4357 (1974).
[63]K. Fruchey and M. D. Fayer, J. Phys. Chem. B **114**, 2840-2845 (2010).
[64]C. Lawler and M. D. Fayer, J. Phys. Chem. B **117**, 9768-9774 (2013).
[65]D. Laage and J. T. Hynes, Science **311**, 832-835 (2006).
[66]D. Laage and J. T. Hynes, J. Phys. Chem. B **112**(45), 14230-14242 (2008).
[67]A. L. Sturlaugson, K. S. Fruchey, and M. D. Fayer, J. Phys. Chem. B **116**, 1777-1787 (2012).
[68]R. B. Williams, R. F. Loring, and M. D. Fayer, J. Phys. Chem. B **105**, 4068-4071 (2001).

This article is copyrighted as indicated in the article. Reuse of AIP content is subject to the terms at: http://scitation.aip.org/termsconditions. Downloaded to IP: 171.64.123.74 On: Wed, 18 Mar 2015 16:17:11